Published in final edited form as:

Sci Transl Med. 2014 September 17; 6(254): 254ra125. doi:10.1126/scitranslmed.3009448.

Tumor clone dynamics in lethal prostate cancer

Suzanne Carreira[1,*], **Alessandro Romanel**[2,*], **Jane Goodall**[1,*], **Emily Grist**[1,3], **Roberta Ferraldeschi**[1,3], **Susana Miranda**[1], **Davide Prandi**[2], **David Lorente**[1,3], **Jean-Sebastien Frenel**[1], **Carmel Pezaro**[1,3], **Aurelius Omlin**[1,3], **Daniel Nava Rodrigues**[1], **Penelope Flohr**[1], **Nina Tunariu**[1,3], **Johann S. de Bono**[1,3], **Francesca Demichelis**[2,4,5,†,‡], and **Gerhardt Attard**[1,3,†,‡]

[1]The Institute of Cancer Research, London SM2 5NG, UK

[2]Centre for Integrative Biology, University of Trento, Trento 38123, Italy

[3]Royal Marsden National Health Service Foundation Trust, London SM2 5PT, UK

[4]Institute for Computational Biomedicine, Weill Cornell Medical College, New York, NY 10021, USA

[5]Institute for Precision Medicine, Weill Cornell Medical College, New York, NY 10021, USA

Abstract

It is unclear whether a single clone metastasizes and remains dominant over the course of lethal prostate cancer. We describe the clonal architectural heterogeneity at different stages of disease progression by sequencing serial plasma and tumor samples from 16 *ERG*-positive patients. By characterizing the clonality of commonly occurring deletions at 21q22, 8p21, and 10q23, we identified multiple independent clones in metastatic disease that are differentially represented in tissue and circulation. To exemplify the clinical utility of our studies, we then showed a temporal association between clinical progression and emergence of androgen receptor (AR) mutations activated by glucocorticoids in about 20% of patients progressing on abiraterone and prednisolone

‡Corresponding author. gerhardt.attard@icr.ac.uk (G.A.); demichelis@science.unitn.it (F.D.).
*These authors contributed equally to this work.
†Co-senior authors.

Supplementary Materials: www.sciencetranslationalmedicine.org/cgi/content/full/6/254/254ra125/DC1

Author contributions: S.C. and J.G. performed all the DNA extractions, sequencing, luciferase reporter assays, and digital PCR experiments. A.R. and F.D. analyzed the data with input from S.C, J.G., E.G., D.P., and G.A. S.M. performed the FISH experiments and scored them with G.A. S.C, A.R., F.D., and G.A. designed the sequencing panel. S.C., J.G., and J.-S.F. developed the sequencing assay. E.G., R.F., D.L, C.P., A.O., P.F., J.S.d.B, and GA contributed patients and obtained samples. NT. performed radiologically guided biopsies, and D.N.R. identified areas of tumor in samples. J.S.d.B, F.D., and G.A. obtained funding. F.D. and G.A. were responsible for overall project design and interpretation of data and wrote the manuscript. All authors read and approved the final manuscript.

Competing interests: The ICR developed abiraterone and therefore has a commercial interest in this agent. G.A. is on the ICR list of rewards to inventors for abiraterone. J.S.d.B. has received consulting fees and travel support from Amgen, Astellas, AstraZeneca, Boehringer Ingelheim, Bristol-Myers Squibb, Dendreon, Enzon, Exelixis, Genentech, GlaxoSmithKline, Mediation, Merck, Novartis, Pfizer, Roche, Sanofi-Aventis, Supergen, and Takeda and grant support from AstraZeneca and Genentech. G.A. has received honoraria, consulting fees or travel support from Astellas, Medivation, Janssen, Millennium Pharmaceuticals, Ipsen, Takeda, and Sanofi-Aventis and grant support from Janssen, AstraZeneca, and Genentech. A.O. serves on advisory boards for Janssen, Astellas, Bayer, and AstraZeneca. F.D. is co-inventor of the patent on the detection of gene fusions in prostate cancer, filed by the University of Michigan and the Brigham and Women's Hospital. The diagnostic field of use for ETS gene fusions has been licensed to Hologic Gen-Probe.

Data and materials availability: The code used in this study can be obtained for academic use upon request.

or dexamethasone. Resistant clones showed a complex dynamic with temporal and spatial heterogeneity, suggesting distinct mechanisms of resistance at different sites that emerged and regressed depending on treatment selection pressure. This introduces a management paradigm requiring sequential monitoring of advanced prostate cancer patients with plasma and tumor biopsies to ensure early discontinuation of agents when they become potential disease drivers.

Introduction

Studies in prostate cancer have suggested paths of tumor evolution inferred from the genomic profiles of tissue specimens from multiple patients (1) or from multiple sites from one individual (2). Several studies have identified commonly occurring chromosomal rearrangements and copy number losses intumors before the start of endocrine treatment (3, 4). These include deletions involving 21q22 [invariably associated with an ERG gene fusion (5, 6)], *NKX3.1* on 8p21, and *PTEN* on 10q23 (4, 7). A single prostate often contains territorially distinct foci with clonal distribution of 21q22 and 8p21 deletions that putatively occurred early in the development of that clone (1, 8, 9). Patients diagnosed with prostate cancer demonstrate highly variable clinical behavior, with a large number of tumors not progressing after decades of observation. Tumors are risk-stratified on the basis of clinical and pathological features, but foci with fewer aggressive features than adjacent areas may give rise to distant and lethal metastases (10). It is therefore unclear whether multiple foci with different genomic patterns at diagnosis metastasize and give rise to the lethal phenotype or a single clone maintains dominance over the course of the disease. Sequential sampling of prostate cancer could shed light on this. However, collection of repeated tumor biopsies is challenging. Moreover, castration-resistant prostate cancer (CRPC) biopsies of one region may not be reflective of other genomically heterogeneous metastases. Tumor DNA circulates in plasma from advanced cancer patients and can be sequentially collected for monitoring of changes in tumor status (11–14). The mechanisms underlying entry of tumor DNA into circulation are uncertain, but circulating genomic material may arise from multiple distinct metastases. Changes in allelic frequency of tumor-specific aberrations relative to total circulating DNA have shown a strong correlation with clinical outcome in several epithelial malignancies (11). This offers an important opportunity for monitoring the dynamics of common aberrations over the course of lethal prostate cancer. However, because recurrent somatic point mutations (commonly involving *SPOP*, *TP53*, and *FOXA1*) occur in at most 20% of prostate cancers (3, 7), strategies for copy number estimation are required to broadly allow quantitation of circulating tumor content.

Most metastatic prostate cancer patients respond to castration alone or with first-generation antiandrogens such as bicalutamide. However, CRPC almost invariably develops after a median of about 18 months. Androgen receptor (AR) amplification or mutations are reported after development of castration resistance, but rarely before endocrine treatment, suggesting that treatment resistance can occur secondary to genomic adaptations that maintain AR signaling (7, 15, 16). The efficacy reported with second-generation endocrine treatments that potently antagonize AR or target androgen synthesis confirms that AR remains a critical driver in a substantial proportion of CRPC patients (17). There is now an urgent need to identify tumor adaptations that underlie resistance to repeated AR targeting in CRPC. By

serially evaluating the clonal evolution of tumor aberrations that commonly occur in prostate cancer (Fig. 1), we aimed to establish a strategy for monitoring tumor dynamics and identifying genomic causes of resistance that demonstrate a temporal association with clinical progression.

Results

Strategy for tumor fractionation and copy number estimation by targeted deep sequencing of circulating DNA

Taking advantage of strategies developed for estimating tumor purity and lesion hierarchy from whole-genome sequencing (1), we aimed to leverage the genetic information of single individuals at heterozygous single-nucleotide polymorphisms (SNPs), informative SNPs, to computationally determine the fraction of total DNA in circulation that contained common monoallelic deletions (see Supplementary Materials and Methods). We hypothesized that combining this approach with copy number assessments and point mutation detection would allow us to follow tumor content and relative abundance of somatic genomic lesions of genes of interest. Although whole-exome/genome sequencing is feasible on patients with advanced cancer when sufficient tumor DNA is present in circulation (18, 19), targeted deep-sequencing achieving high coverage with lower input DNA currently allows applicability across a broader range of patients, including men with lower-volume metastatic disease. We therefore designed a custom panel to deep-sequence 38,752 bases at high coverage, with input DNA as low as 6 ng. We included all the coding exons of *SPOP*, *TP53*, *FOXA1*, and *PTEN*. To detect deletions at 21q22, 8p21, and 10q23, we included at least 50 SNPs with a high variant allele frequency across each region (table S1).

To calculate the performance of our targeted sequencing and computational approach strategy, we first sequenced plasma from male, age-matched healthy volunteers. To measure point mutation detection performances, we generated simulated data for different combinations of allelic fraction, tumor content, and coverage. For 10% allelic fractions, the analyses demonstrated precision (positive predictive value) ≥80% across the majority of coverage ranges in the presence of high tumor content and about 60% for tumor content at 20%. For 20% allelic fractions, precision scored above 95% across all tumor content levels (fig. S1). All false discovery rates were below 1%. A similar strategy was implemented to measure the performance of monoallelic deletion detection. Mean sensitivity and mean specificity around 90 and 83%, respectively, were achieved for percentages of aberrant tumor reads around 10% (for 50 or more informative SNPs and minimum mean coverage of 1000×) (Fig. 2A). Mean sensitivity and specificity above 98% were achieved for aberrant tumor reads above 15%. Supplementary Materials and Methods and fig. S2 present the details of this analysis.

Detection of common tumor aberrations in sequential plasma samples from *ERG*-positive lethal prostate cancer

To enrich for metastatic CRPC patients with a common deletion, we selected 16 *ERG*-positive patients detected by break-apart fluorescence in situ hybridization (FISH) on tumor sections. All 16 patients were treated with the specific CYP17A1 inhibitor abiraterone (20),

and 5 also received the potent antiandrogen enzalutamide (21), both of which are now licensed for the treatment of metastatic CRPC (Table 1 and table S2). We used our targeted panel to sequence germ-line DNA from these patients, and 106 sequential plasma samples, CRPC tumor biopsies (n = 14 from 7 patients), and multiple precastration tumor cores (n = 33 from 12 patients, maximum of 4 per patient) obtained at diagnostic transrectal biopsy or prostatectomy (table S3; for read depth coverage, see table S4).

We confirmed detection of deletion at 21q22.2 to 21q22.3 in tumors (precastration or CRPC) from all 16 patients, including 3 patients who showed rearrangement but preservation of the 5′ probe (Fig. 2B). By sequencing multiple precastration cores, we also detected 8p21 loss involving *NKX3.1* and 10q23 loss involving *PTEN* in 11 of 12 patients (Fig. 2B). We observed 100% concordance between detection of 21q22 deletion in precastration samples and CRPC plasma (Fig. 2C). Deletions at 8p21 and 10q23 identified before castration were detected in 90 and 100% of CRPC plasma samples, respectively, and they were found in 90 and 92% of precastration samples, respectively, when detected in CRPC plasma (Fig. 2C).

We detected point mutations involving *TP53* and *FOXA1* in pre-castration samples from 3 of 16 and 1 of 16 patients, respectively (Fig. 2D and table S5). We used digital droplet polymerase chain reaction (PCR) to validate selected point mutations (fig. S3). Our targeted sequencing strategy allowed us to follow these point mutations over the course of CRPC, and we observed a 100% concordance with detection in CRPC plasma, suggesting that these are early events that remain present in later metastatic clones. We noted deletion of the second *TP53* allele in samples with a *TP53* mutation, validated by digital droplet PCR (fig. S4). We also detected a *PTEN* point mutation in CRPC plasma from 1 of 16 patients, although the precastration tissue was not available for comparison (Fig. 2D and table S5). We did not detect *SPOP* mutations, but we observed copy number gain of *SPOP* in 8 of 47 tumor samples from 7 patients (4 of 33 precastrations and 4 of 14 CRPCs). Further investigation in two independent data sets of CRPC (4, 7) demonstrated nonfocal gains spanning *SPOP* in about 30% of CRPCs (table S6).

We used the dominant tumor lesion(s) at each time point to estimate circulating tumor content (table S7). This explained the high total circulating DNA in most nonresponders, although we observed discordance at progression in a subgroup of responders who had increased total circulating DNA but a relatively low fraction of targeted deletions and mutations (Fig. 2E). Similarly, we observed that a high circulating tumor cell (CTC) count was associated with high estimated tumor content in most patients (Fig. 2F).

Dynamics of relative abundance of common tumor deletions

Next, we evaluated clonality in multiple cores acquired before initiation of castration, and we detected different combinations of loss of 21q22, 10q23, and 8p21 in the same prostate (Fig. 3 and table S8). FISH and immunohistochemistry studies (8, 22) suggest that this is a result of mixture of both *ERG*-positive and *ERG*-negative foci in the same core. To evaluate whether progression after castration and subsequent treatments selected for a single dominant clone, we assessed clonality in patient-matched sequential tumor biopsies and plasma samples. Surprisingly, in several patients, clonality was not conserved after

development of metastatic disease, and instead, we observed continuously changing patterns of the relative frequencies of common deletions in sequential plasma samples (Fig. 3). Furthermore, we saw cases where dominant deletions became subclonal or even undetectable altogether with different treatments and then reemerged at a dominant frequency at a later time point. At multiple time points in plasma and tumors, we detected differences in the relative abundance of deletions that had been previously detected at the same frequency. For example, for patient V4048, deletion of 10q23 was the most abundant deletion in circulation before docetaxel chemotherapy (Fig. 3 and fig. S5). He was subsequently treated with abiraterone, and at the point of maximum biochemical and clinical response, deletions at 21q22 and 10q23 showed equal abundance, whereas 8p21 was subclonally deleted. After a further 112 days of treatment, his serum prostate-specific antigen (PSA) started to rise, and all three deletions were equally subclonal. After another 35 days, when he had confirmed radiological and clinical progression, deletion at 8p21 was the most abundant. Another sample before initiation of cabazitaxel showed equal abundance of 21q22 and 8p21 loss. We also observed a decrease in the fraction of tumor lesions with treatment that is in keeping with data from previous studies in other malignancies (11). Comparison of synchronously collected plasma DNA and CRPC tumor biopsies showed differences in the relative frequencies of deletions (patients V4045 and V5086, identified by surrounding gray border; Fig. 3), further supporting the presence of independent tumor clones in distinct metastases that are differentially represented in circulation.

Emergence of functionally active *AR* mutations in patients receiving exogenous glucocorticoids

To evaluate clonal evolution of aberrations that cause treatment resistance and occur later in the disease course, we also sequenced all the coding exons of the *AR*. We detected mutations only in the ligand-binding domain, in four patients (Fig. 2D). We observed emergence of an *AR-L702H* mutant clone in two patients receiving treatment with an exogenous glucocorticoid: in V4012, in plasma while also on treatment with enzalutamide (Fig. 4A), and in V4045, clonally in a liver metastasis and subclonally in plasma (at a low frequency of 2%) while also receiving abiraterone (table S5). In V4012, subsequent treatment with abiraterone and prednisolone was associated with primary resistance and a progressive rise in the allelic frequency of the *AR-L702H* mutation (Fig. 4B). A substitution of leucine to histidine at position 702 results in increased activation by glucocorticoids in preference to androgens (23). Because this point mutation emerged when the patient was receiving enzalutamide in combination with a glucocorticoid and because enzalutamide was developed through an iterative process, starting with an androgenic scaffold (21), we hypothesized that an *L702H* mutation would result in reduced antagonism in the presence of glucocorticoids. We used AR luciferase reporter assays (fig. S6) to confirm that prednisolone activated *AR-L702H* but not wild-type *AR* and that activation by prednisolone at ≥100 nM (median serum concentration of prednisolone in patients is 152 nM) was not inhibited by enzalutamide (Fig. 4C) (24). To confirm that the increasing frequency of this point mutation was not solely an effect of increasing tumor DNA in circulation, we report the allelic fraction corrected for tumor content estimated using dominant lesions (Fig. 4A). This method identified tumor clones that do not harbor this specific mutation, suggesting other coexistent mechanisms of resistance.

In V5074, we detected an *AR-H875Y* mutation (25% of circulating tumor fraction) at progression after prednisolone alone, but it regressed from circulation after addition of abiraterone and prednisolone, in line with loss of detection of other tumor aberrations. An *AR-H875Y* mutation was detected in one of three pretreatment cores from this case (table S5), suggesting that selection of preexisting *AR* point mutations can underlie resistance in some patients. At progression on abiraterone and prednisolone, *H875Y* and *T878A AR* mutations were both detected, and these persisted after the next line of treatment with cabazitaxel chemotherapy administered with prednisolone (Fig. 4D). The temporal and proportion differences suggest that these two mutations emerged separately. They have been previously shown to be activated by glucocorticoids or 21-carbon steroids, such as progesterone (25), which can remain present at increased levels in patients on abiraterone (20).

AR copy number gain in plasma from CRPC patients

After preprocessing the data to maximize the signal-to-noise ratio and normalizing the signal against the patients' matched germ-line data and control genes, we quantitated *AR* copy number from sequencing data (see Supplementary Materials and Methods). We first confirmed concordance between *AR* copy number gain estimated by deep-sequencing and digital droplet PCR (Fig. 5A, fig. S3, and table S9). We then corrected the observed *AR* copy number in circulating DNA for tumor content, estimated using the dominant genomic aberration (Fig. 5B and table S10). As expected, *AR* copy number gain was detected in only two precastration samples (6%) but in 37 of 106 (35%) and 8 of 14 (57%) of CRPC plasma and tumor samples, respectively. We also observed an association between high copy number of *AR* in circulation and absence of response to abiraterone (Fig. 5C).

Spatial and temporal heterogeneity of *AR* aberrations

In case V5086, we detected an *AR-W742C* mutation [previously reported to be activated by bicalutamide (16, 26)] in an enlarging liver metastasis that developed 3 months after addition of bicalutamide to castration for a rising PSA. This mutation occurred at a frequency equivalent to deletions of *NKX3.1* and *PTEN* and an *A159D-TP53* mutation. Deletions of *NKX3.1* and *PTEN* and the *A159D-TP53* mutation were detected in synchronously collected circulating DNA, but *AR* was wild type at position 742. Also, in contrast to the liver biopsy, circulating tumor DNA contained *AR* amplification (Fig. 6). This patient was treated with docetaxel chemotherapy, to which he had a response in his liver metastases, and subsequently with abiraterone, to which he did not respond. We sequenced DNA from multiple subsequent plasma samples and also a second biopsy from a recurrent liver metastasis and detected *AR* amplification but no base substitution at *AR* position 742, suggesting regression of the *W742C*-mutant clone. A withdrawal response associated with a decline in PSA is described in about 15% of patients after bicalutamide discontinuation, putatively explained by the presence of *AR* point mutations such as the *W742C* mutation described here (27). A PSA decline was not manifested in this patient possibly because of the concurrent emergence of other clones, including tumor with high *AR* copy number gain.

Discussion

We describe the presence and dynamics of multiple independent tumor clones in lethal prostate cancer, in some patients characterized by distinctly different and continuously changing proportions of genomic loss at 21q22, 8p21, and 10q23 (Fig. 7A). An alternative explanation for changes in abundance of deletions over time is gain of the residual allele in the presence of a monoallelic deletion. However, this is very unlikely given the observed diversity, with dominant deletions becoming subclonal and subsequently dominant again. The different combinations of genomic aberrations in plasma DNA suggest that distinct metastases are differentially and dynamically represented in circulation. This is supported by the detection of point mutations in metastases but not circulating tumor DNA and vice versa, as well as differences in clonality of common deletions in these synchronously collected samples. We are unable to differentiate whether the clonal heterogeneity we observe is a result of multiple different foci with distinct cells of origin or clones arising from the same cell in which these genomic aberrations have occurred stochastically. Although there is an association between *ERG* rearrangement and *PTEN* deletion (28, 29), here we identified a higher prevalence of loss of *PTEN* and *NKX3.1* than reported previously. The detection of coexistent clones, each with a different *ERG* status, is in contrast to previous studies on metastases obtained at rapid autopsy or CTC data that reported 21q deletion in all CRPC tissue from the same patient (2, 30). These two findings could be explained by the greater sensitivity achieved by sequential plasma and tumor biopsy next-generation sequencing, although the high prevalence of loss of *PTEN* and *NKX3.1* could also be due to the selection of patients who all developed lethal CRPC.

Our strategy for detecting monoallelic deletions was limited to aberrations occurring at a minimum of about 10% of total circulating DNA. Therefore, no deletions were detected at several time points (Fig. 3). Improvements in the assay design could achieve a lower threshold and allow detection of deletions in patients with less circulating tumor DNA. Second, evaluation of larger cohorts of patients is now required to more accurately understand the prevalence of our observations and measure the predictive value of genomic lesions in terms of treatment response. Third, underestimation of circulating tumor content is a limitation of targeted sequencing strategies such as ours because of the possible emergence of clones harboring less common genomic aberrations that are not tested for. Sequencing of additional regions, including regions covering genomic aberrations identified in ongoing prospective next-generation sequencing studies of large numbers of CRPC tumor biopsies, will mitigate this risk.

Also, a targeted approach does not efficiently detect new mechanisms of resistance but is designed to confirm clinical associations with putative resistance-causing aberrations. Here, we describe a temporal relationship between the emergence of *AR* point mutations and clinical progression on abiraterone or enzalutamide in three patients also receiving exogenous glucocorticoids (Fig. 7B). We confirmed that emergence of the *AR-L702H* mutation could result in activation of AR signaling that would not be inhibited by enzalutamide. This observation could explain cross-resistance between abiraterone and enzalutamide in some postchemotherapy patients, who commonly continued glucocorticoids with enzalutamide (31–33). Additionally, it could have implications for ongoing clinical

trials evaluating the combination of enzalutamide, abiraterone, and prednisolone. This scenario introduces the possibility of a patient-management paradigm whereby administration of glucocorticoids or other agents shown to activate an emergent *AR* aberration is avoided or replaced by treatment with activity against the mutant clone.

In our five patients who received and progressed on enzalutamide, we did not detect the *AR-F876L* mutation previously reported in plasma from patients progressing on the antiandrogen ARN-509 (34) and also shown to be activated by enzalutamide (35). We have also shown evidence, in circulating DNA and tumor biopsies, of regression of independent tumor clones and a clone containing an *AR-W742C* mutation associated with resistance to bicalutamide. This has implications for interpreting genomic causes of treatment resistance when an intervening treatment has been administered. Our strategy of reporting *AR* mutations as a proportion of circulating tumor content rather than total circulating DNA allowed us to demonstrate that point mutations are not present in all progressing tumor clones. In some patients, we detected *AR* copy number gain and point mutations independently in the same patient, suggesting that resistance occurred secondary to activation of *AR* through independent mechanisms. In conclusion, our study demonstrates the translational relevance of studies on sequential tumor biopsies and circulating DNA as a tool for monitoring complex clone dynamics and genomic causes of treatment resistance in prostate cancer.

Materials and Methods

Study design

We aimed to study the dynamics of common genomic aberrations in sequential plasma and tumor samples from *ERG*-positive CRPC patients who received treatment with abiraterone. Up to 20 ml of blood was collected from each patient at multiple time points, up to a maximum of eight times per year, from development of castration resistance to after discontinuation of abiraterone. Plasma was extracted and frozen within 2 hours. Archived formalin-fixed paraffin-embedded (FFPE) blocks were obtained from pathology archives. FISH to identify *ERG*-positive patients was performed and scored as described previously (30). Patients provided informed consent and understood the nature and implications of the study. Sample collection for this study was approved by The Royal Marsden (London, UK) Research Ethics Committee (REC 04/Q0801/6) and by The Royal Marsden Committee for Clinical Research. Patients were defined as responders to abiraterone and prednisolone if a more than 50% decline in PSA from baseline was demonstrated after a minimum of 12 weeks of treatment or there was evidence of a radiological response as defined previously (20). Enumeration of CTC was performed with the CellSearch (Veridex) platform.

DNA extraction and quantification

Buccal swab and FFPE DNA were extracted with the QIAamp DNA and FFPE Tissue DNA kits (Qiagen), respectively. Circulating DNA was extracted from 2 ml of plasma with the SnoMag Circulating DNA kit (Snova Biotechnologies) according to the manufacturer's protocol and quantified with the Quant-iT high-sensitivity PicoGreen double-stranded DNA Assay Kit (Invitrogen).

Deep sequencing

Amplicon coordinates are listed in table S11. We used 6 ng of circulating DNA to generate libraries with the Ion AmpliSeq library preparation kit v2.0 (Life Technologies), according to the manufacturer's protocol. Libraries were sequenced on the PGM Ion Torrent (Life Technologies) with a PGM 200 sequencing kit v2 and 318 Chip v2. A maximum of eight libraries were pooled to achieve at least 1000× coverage per target amplicon.

Sequencing data analysis, tumor content, and clonality

Genotypes of study SNPs were determined from the germ-line samples to compile the list of informative SNPs for each patient (SNPs where the individual has heterozygous calls). Point mutations for tumor samples were identified by applying strict filtering procedures on coverage, allelic fraction, and genomic position. Validation was performed by digital PCR (described in Supplementary Materials and Methods). Tumor content and clonality for all tumor samples were estimated with an ad hoc procedure to specifically deal with target sequencing data from low tumor content samples integrated with the CLONET framework developed by our group at the University of Trento, Italy (36). Details are reported in Supplementary Materials and Methods.

Somatic copy number aberration detection

For 21q, 8p, and 10q genomic regions, CLONET estimates were used to identify monoallelic losses. Confidence and error estimates were computed using simulated data. In addition, we developed an ad hoc read-depth method to assess the copy number state of the genes of interest represented on the targeted sequencing assay. Data preprocessing identified the set of amplicons with favorable signal-to-noise ratios across all patients' germ-line data. We then used selected amplicons to compute the $\log_2$ ratio between normalized tumor amplicon signal and normalized germ-line amplicon signal for each gene. Normalization was sample-based and used a subset of assay genes as reference. Details are discussed in Supplementary Materials and Methods.

Luciferase reporter assays

We constructed a PSA-ARE3-luc luciferase reporter plasmid that was cotransfected with a human AR expression plasmid, F527-AR [wild type or L702H; mutation confirmed by sequencing (Beckman Coulter Genomics)] into PC-3 cells as described previously (24). Luciferase activity was determined by adding ONE-Glo (Promega) and measuring luminescence on a TopCount plate reader (PerkinElmer).

Supplementary Material

Refer to Web version on PubMed Central for supplementary material.

Acknowledgments

We thank the participating men and their families who suffered from metastatic prostate cancer and nonetheless gave the gift of participation so that others might benefit.

Funding: This work was funded by Prostate Cancer UK PG12-49, Cancer Research UK A13239, National Cancer Institute grant R01 CA116337-06A1, Department of Defense PC101020P2, and the Prostate Cancer Foundation. D.L was supported by a fellowship from the Spanish Medical Oncology Society "Beca SEOM para la Investigacion Traslacional en el Extranjero." A.O. was supported by a grant from the Swiss Cancer League (BIL KLS-02592-02-2010). G.A. is a Cancer Research UK clinician scientist. We also acknowledge National Institute for Health Research funding to The Royal Marsden/Institute of Cancer Research (ICR) Biomedical Research Centre.

References and Notes

1. Baca SC, Prandi D, Lawrence MS, Mosquera JM, Romanel A, Drier Y, Park K, Kitabayashi N, MacDonald TY, Ghandi M, Van Allen E, Kryukov GV, Sboner A, Theurillat JP, Soong TD, Nickerson E, Auclair D, Tewari A, Beltran H, Onofrio RC, Boysen G, Guiducci C, Barbieri CE, Cibulskis K, Sivachenko A, Carter SL, Saksena G, Voet D, Ramos AH, Winckler W, Cipicchio M, Ardlie K, Kantoff PW, Berger MF, Gabriel SB, Golub TR, Meyerson M, Lander ES, Elemento O, Getz G, Demichelis F, Rubin MA, Garraway LA. Punctuated evolution of prostate cancer genomes. Cell. 2013; 153:666–677. [PubMed: 23622249]
2. Liu W, Laitinen S, Khan S, Vihinen M, Kowalski J, Yu G, Chen L, Ewing CM, Eisenberger MA, Carducci MA, Nelson WG, Yegnasubramanian S, Luo J, Wang Y, Xu J, Isaacs WB, Visakorpi T, Bova GS. Copy number analysis indicates monoclonal origin of lethal meta-static prostate cancer. Nat Med. 2009; 15:559–565. [PubMed: 19363497]
3. Barbieri CE, Baca SC, Lawrence MS, Demichelis F, Blattner M, Theurillat JP, White TA, Stojanov P, Van Allen E, Stransky N, Nickerson E, Chae SS, Boysen G, Auclair D, Onofrio RC, Park K, Kitabayashi N, MacDonald TY, Sheikh K, Vuong T, Guiducci C, Cibulskis K, Sivachenko A, Carter SL, Saksena G, Voet D, Hussain WM, Ramos AH, Winckler W, Redman MC, Ardlie K, Tewari AK, Mosquera JM, Rupp N, Wild PJ, Moch H, Morrissey C, Nelson PS, Kantoff PW, Gabriel SB, Golub TR, Meyerson M, Lander ES, Getz G, Rubin MA, Garraway LA. Exome sequencing identifies recurrent SPOP, FOXA1 and MED12 mutations in prostate cancer. Nat Genet. 2012; 44:685–689. [PubMed: 22610119]
4. Demichelis F, Setlur SR, Beroukhim R, Perner S, Korbel JO, Lafargue CJ, Pflueger D, Pina C, Hofer MD, Sboner A, Svensson MA, Rickman DS, Urban A, Snyder M, Meyerson M, Lee C, Gerstein MB, Kuefer R, Rubin MA. Distinct genomic aberrations associated with ERG rearranged prostate cancer. Genes Chromosome Cancer. 2009; 48:366–380.
5. Tomlins SA, Rhodes DR, Perner S, Dhanasekaran SM, Mehra R, Sun XW, Varambally S, Cao X, Tchinda J, Kuefer R, Lee C, Montie JE, Shah RB, Pienta KJ, Rubin MA, Chinnaiyan AM. Recurrent fusion of TMPRSS2 and ETS transcription factor genes in prostate cancer. Science. 2005; 310:644–648. [PubMed: 16254181]
6. Perner S, Demichelis F, Beroukhim R, Schmidt FH, Mosquera JM, Setlur S, Tchinda J, Tomlins SA, Hofer MD, Pienta KG, Kuefer R, Vessella R, Sun XW, Meyerson M, Lee C, Sellers WR, Chinnaiyan AM, Rubin MA. TMPRSS2:ERG fusion-associated deletions provide insight into the heterogeneity of prostate cancer. Cancer Res. 2006; 66:8337–8341. [PubMed: 16951139]
7. Grasso CS, Wu YM, Robinson DR, Cao X, Dhanasekaran SM, Khan AP, Quist MJ, Jing X, Lonigro RJ, Brenner JC, Asangani IA, Ateeq B, Chun SY, Siddiqui J, Sam L, Anstett M, Mehra R, Prensner JR, Palanisamy N, Ryslik GA, Vandin F, Raphael BJ, Kunju LP, Rhodes DR, Pienta KJ, Chinnaiyan AM, Tomlins SA. The mutational landscape of lethal castration-resistant prostate cancer. Nature. 2012; 487:239–243. [PubMed: 22722839]
8. Clark J, Attard G, Jhavar S, Flohr P, Reid A, De-Bono J, Eeles R, Scardino P, Cuzick J, Fisher G, Parker MD, Foster CS, Berney D, Kovacs G, Cooper CS. Complex patterns of ETS gene alteration arise during cancer development in the human prostate. Oncogene. 2008; 27:1993–2003. [PubMed: 17922029]
9. Cheng L, Song SY, Pretlow TG, Abdul-Karim FW, Kung HJ, Dawson DV, Park WS, Moon YW, Tsai ML, Linehan WM, Emmert-Buck MR, Liotta LA, Zhuang Z. Evidence of independent origin of multiple tumors from patients with prostate cancer. J Natl Cancer Inst. 1998; 90:233–237. [PubMed: 9462681]
10. Haffner MC, Mosbruger T, Esopi DM, Fedor H, Heaphy CM, Walker DA, Adejola N, Gürel M, Hicks J, Meeker AK, Halushka MK, Simons JW, Isaacs WB, De Marzo AM, Nelson WG,

Yegnasubramanian S. Tracking the clonal origin of lethal prostate cancer. J Clin Invest. 2013; 123:4918–4922. [PubMed: 24135135]

11. Dawson SJ, Tsui DW, Murtaza M, Biggs H, Rueda OM, Chin SF, Dunning MJ, Gale D, Forshew T, Mahler-Araujo B, Rajan S, Humphray S, Becq J, Halsall D, Wallis M, Bentley D, Caldas C, Rosenfeld N. Analysis of circulating tumor DNA to monitor metastatic breast cancer. N Engl J Med. 2013; 368:1199–1209. [PubMed: 23484797]
12. Diehl F, Li M, Dressman D, He Y, Shen D, Szabo S, Diaz LA Jr, Goodman SN, David KA, Juhl H, Kinzler KW, Vogelstein B. Detection and quantification of mutations in the plasma of patients with colorectal tumors. Proc Natl Acad Sci U S A. 2005; 102:16368–16373. [PubMed: 16258065]
13. Bettegowda C, Sausen M, Leary RJ, Kinde I, Wang Y, Agrawal N, Bartlett BR, Wang H, Luber B, Alani RM, Antonarakis ES, Azad NS, Bardelli A, Brem H, Cameron JL, Lee CC, Fecher LA, Gallia GL, Gibbs P, Le D, Giuntoli RL, Goggins M, Hogarty MD, Holdhoff M, Hong SM, Jiao Y, Juhl HH, Kim JJ, Siravegna G, Laheru DA, Lauricella C, Lim M, Lipson EJ, Marie SK, Netto GJ, Oliner KS, Olivi A, Olsson L, Riggins GJ, Sartore-Bianchi A, Schmidt K, Shih IM, Oba-Shinjo SM, Siena S, Theodorescu D, Tie J, Harkins TT, Veronese S, Wang TL, Weingart JD, Wolfgang CL, Wood LD, Xing D, Hruban RH, Wu J, Allen PJ, Schmidt CM, Choti MA, Velculescu VE, Kinzler KW, Vogelstein B, Papadopoulos N, Diaz LA Jr. Detection of circulating tumor DNA in early- and late-stage human malignancies. Sci Transl Med. 2014; 6:224ra24.
14. Forshew T, Murtaza M, Parkinson C, Gale D, Tsui DW, Kaper F, Dawson SJ, Piskorz AM, Jimenez-Linan M, Bentley D, Hadfield J, May AP, Caldas C, Brenton JD, Rosenfeld N. Noninvasive identification and monitoring of cancer mutations by targeted deep sequencing of plasma DNA. Sci Transl Med. 2012; 4:136ra68.
15. Visakorpi T, Hyytinen E, Koivisto P, Tanner M, Keinänen R, Palmberg C, Palotie A, Tammela T, Isola J, Kallioniemi OP. In vivo amplification of the androgen receptor gene and progression of human prostate cancer. Nat Genet. 1995; 9:401–406. [PubMed: 7795646]
16. Taplin ME, Bubley GJ, Shuster TD, Frantz ME, Spooner AE, Ogata GK, Keer HN, Balk SP. Mutation of the androgen-receptor gene in metastatic androgen-independent prostate cancer. N Engl J Med. 1995; 332:1393–1398. [PubMed: 7723794]
17. Attard G, Cooper CS, de Bono JS. Steroid hormone receptors in prostate cancer: A hard habit to break? Cancer Cell. 2009; 16:458–462. [PubMed: 19962664]
18. Murtaza M, Dawson SJ, Tsui DW, Gale D, Forshew T, Piskorz AM, Parkinson C, Chin SF, Kingsbury Z, Wong AS, Marass F, Humphray S, Hadfield J, Bentley D, Chin TM, Brenton JD, Caldas C, Rosenfeld N. Non-invasive analysis of acquired resistance to cancer therapy by sequencing of plasma DNA. Nature. 2013; 497:108–112. [PubMed: 23563269]
19. Leary RJ, Sausen M, Kinde I, Papadopoulos N, Carpten JD, Craig D, O'Shaughnessy J, Kinzler KW, Parmigiani G, Vogelstein B, Diaz LA Jr, Velculescu VE. Detection of chromosomal alterations in the circulation of cancer patients with whole-genome sequencing. Sci Transl Med. 2012; 4:162ra154.
20. Attard G, Reid AH, Yap TA, Raynaud F, Dowsett M, Settatree S, Barrett M, Parker C, Martins V, Folkerd E, Clark J, Cooper CS, Kaye SB, Dearnaley D, Lee G, de Bono JS. Phase I clinical trial of a selective inhibitor of CYP17, abiraterone acetate, confirms that castration-resistant prostate cancer commonly remains hormone driven. J Clin Oncol. 2008; 26:4563–4571. [PubMed: 18645193]
21. Tran C, Ouk S, Clegg NJ, Chen Y, Watson PA, Arora V, Wongvipat J, Smith-Jones PM, Yoo D, Kwon A, Wasielewska T, Welsbie D, Chen CD, Higano CS, Beer TM, Hung DT, Scher HI, Jung ME, Sawyers CL. Development of a second-generation antiandrogen for treatment of advanced prostate cancer. Science. 2009; 324:787–790. [PubMed: 19359544]
22. Barry M, Perner S, Demichelis F, Rubin MA. TMPRSS2-ERG fusion heterogeneity in multifocal prostate cancer: Clinical and biologic implications. Urology. 2007; 70:630–633. [PubMed: 17991527]
23. Zhao XY, Malloy PJ, Krishnan AV, Swami S, Navone NM, Peehl DM, Feldman D. Glucocorticoids can promote androgen-independent growth of prostate cancer cells through a mutated androgen receptor. Nat Med. 2000; 6:703–706. [PubMed: 10835690]
24. Richards J, Lim AC, Hay CW, Taylor AE, Wingate A, Nowakowska K, Pezaro C, Carreira S, Goodall J, Arlt W, McEwan IJ, de Bono JS, Attard G. Interactions of abiraterone, eplerenone, and

prednisolone with wild-type and mutant androgen receptor: A rationale for increasing abiraterone exposure or combining with MDV3100. Cancer Res. 2012; 72:2176–2182. [PubMed: 22411952]

25. Steketee K, Timmerman L, Zielvan der Made AC, Doesburg P, Brinkmann AO, Trapman J. Broadened ligand responsiveness of androgen receptor mutants obtained by random amino acid substitution of H874 and mutation hot spot T877 in prostate cancer. Int J Cancer. 2002; 100:309–317. [PubMed: 12115546]
26. Yoshida T, Kinoshita H, Segawa T, Nakamura E, Inoue T, Shimizu Y, Kamoto T, Ogawa O. Antiandrogen bicalutamide promotes tumor growth in a novel androgen-dependent prostate cancer xenograft model derived from a bicalutamide-treated patient. Cancer Res. 2005; 65:9611–9616. [PubMed: 16266977]
27. Small EJ, Halabi S, Dawson NA, Stadler WM, Rini BI, Picus J, Gable P, Torti FM, Kaplan E, Vogelzang NJ. Antiandrogen withdrawal alone or in combination with ketocona-zole in androgen-independent prostate cancer patients: A phase III trial (CALGB 9583). J Clin Oncol. 2004; 22:1025–1033. [PubMed: 15020604]
28. Reid AH, Attard G, Brewer D, Miranda S, Riisnaes R, Clark J, Hylands L, Merson S, Vergis R, Jameson C, Høyer S, Sørenson KD, Borre M, Jones C, de Bono JS, Cooper CS. Novel, gross chromosomal alterations involving PTEN cooperate with allelic loss in prostate cancer. Mod Pathol. 2012; 25:902–910. [PubMed: 22460813]
29. Fontugne J, Lee D, Cantaloni C, Barbieri CE, Caffo O, Hanspeter E, Mazzoleni G, Dalla Palma P, Rubin MA, Fellin G, Mosquera JM, Barbareschi M, Demichelis F. Recurrent prostate cancer genomic alterations predict response to brachytherapy treatment. Cancer Epidemiol Biomarkers Prev. 2014; 23:594–600. [PubMed: 24515272]
30. Attard G, Swennenhuis JF, Olmos D, Reid AH, Vickers E, A'Hern R, Levink R, Coumans F, Moreira J, Riisnaes R, Oommen NB, Hawche G, Jameson C, Thompson E, Sipkema R, Carden CP, Parker C, Dearnaley D, Kaye SB, Cooper CS, Molina A, Cox ME, Terstappen LW, de Bono JS. Characterization of ERG, AR and PTEN gene status in circulating tumor cells from patients with castration-resistant prostate cancer. Cancer Res. 2009; 69:2912–2918. [PubMed: 19339269]
31. Noonan KL, North S, Bitting RL, Armstrong AJ, Ellard SL, Chi KN. Clinical activity of abiraterone acetate in patients with metastatic castration-resistant prostate cancer progressing after enzalutamide. Ann Oncol. 2013; 24:1802–1807. [PubMed: 23585511]
32. Loriot Y, Bianchini D, Ileana E, Sandhu S, Patrikidou A, Pezaro C, Albiges L, Attard G, Fizazi K, De Bono JS, Massard C. Antitumour activity of abiraterone acetate against metastatic castration-resistant prostate cancer progressing after docetaxel and enzalutamide (MDV3100). Ann Oncol. 2013; 24:1807–1812. [PubMed: 23576708]
33. Bianchini D, Lorente D, Rodriguez-Vida A, Omlin A, Pezaro C, Ferraldeschi R, Zivi A, Attard G, Chowdhury S, de Bono JS. Antitumour activity of enzalutamide (MDV3100) in patients with metastatic castration-resistant prostate cancer (CRPC) pre-treated with docetaxel and abiraterone. Eur J Cancer. 2014; 50:78–84. [PubMed: 24074764]
34. Joseph JD, Lu N, Qian J, Sensintaffar J, Shao G, Brigham D, Moon M, Maneval EC, Chen I, Darimont B, Hager JH. A clinically relevant androgen receptor mutation confers resistance to second-generation antiandrogens enzalutamide and ARN-509. Cancer Discov. 2013; 3:1020–1029. [PubMed: 23779130]
35. Balbas MD, Evans MJ, Hosfield DJ, Wongvipat J, Arora VK, Watson PA, Chen Y, Greene GL, Shen Y, Sawyers CL. Overcoming mutation-based resistance to antiandrogens with rational drug design. Elife. 2013; 2:e00499. [PubMed: 23580326]
36. Prandi D, Baca SC, Romanel A, Barbieri CE, Mosquera JM, Fontugne J, Beltran H, Sboner A, Garraway LA, Rubin MA, Demichelis F. Unraveling the clonal hierarchy of somatic genomic abberrations. Genome Biol. 2014; 15:439. [PubMed: 25160065]

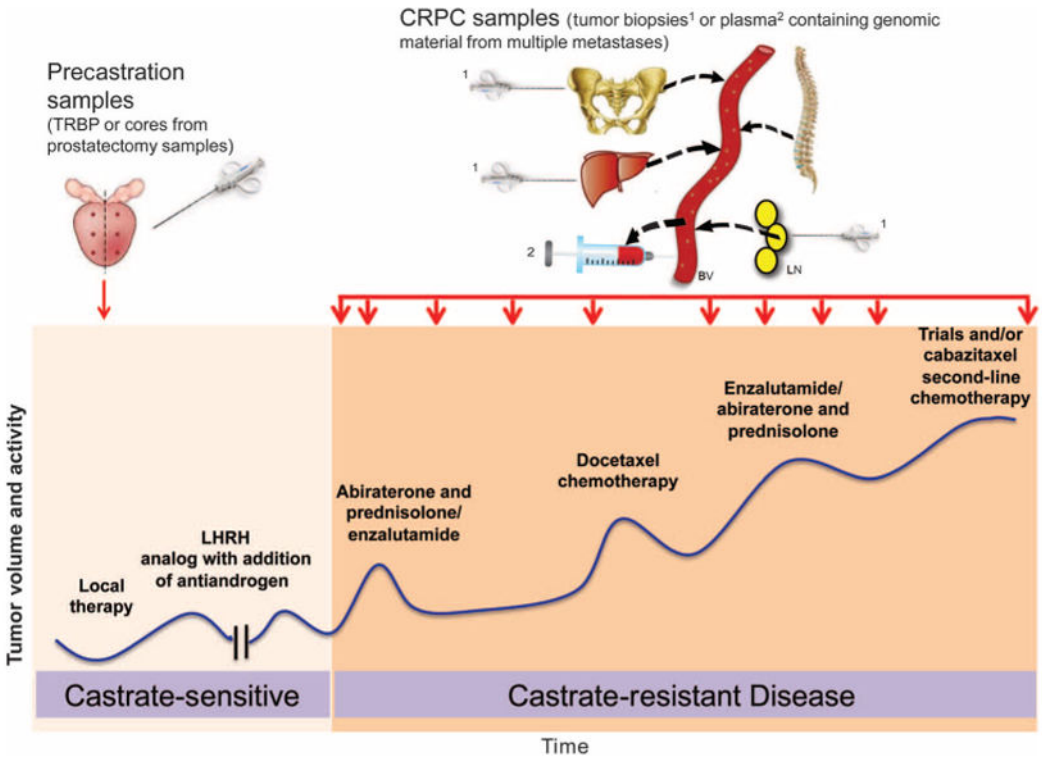

Fig. 1. Strategy for serial evaluation of plasma and tumor samples from prostate cancer patients

Schematic showing change in tumor volume and activity with different treatments and time points at which samples were collected for sequencing. TRBP, transrectal biopsy of the prostate; BV, blood vessel; LN, lymph nodes; LHRH, luteinizing hormone releasing hormone.

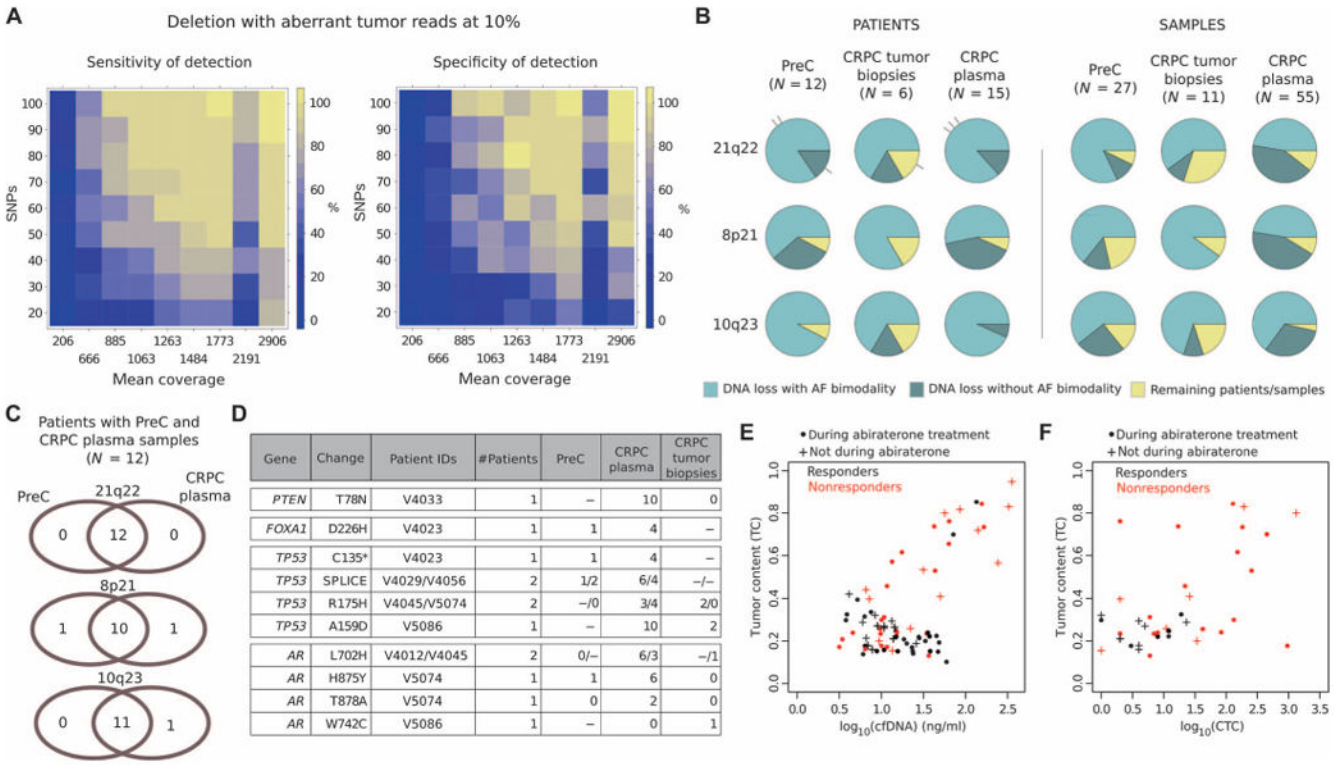

Fig. 2. Detection of genomic lesions in ERG-positive CRPC

(**A**) In silico sensitivity and specificity estimations for monoallelic deletion with aberrant tumor reads at 10%. Each cell in each panel represents a combination of the number of informative SNPs and local mean coverage used to generate the simulated data. (**B**) Distribution of 21q22, 8p21, and 10q23 deletions across patients and samples. Only samples with detected tumor DNA are considered. Gray lines represent patients with an *ERG* gene fusion secondary to rearrangement detected by FISH on tissue. Left panel shows the proportion of patients in whom evidence of loss was detected in at least one sample, grouped by sample type and main genomic lesion. Right panel is the equivalent on a per sample basis. AF, allele frequency. (**C**) For each of the three main deletions, the Venn diagrams indicate the number of patients with evidence of loss in precastration (PreC) samples only, CRPC only, or both. (**D**) Point mutations detected. Cases where no sample was available are identified by "-." (**E** and **F**) Tumor content estimated using the dominant lesion compared to circulating total double-strand DNA (E) and CTC count per 7.5 ml of blood (F). Samples collected on or off treatment with abiraterone and from patients who did or did not have a response to abiraterone are distinguished as shown in the figure.

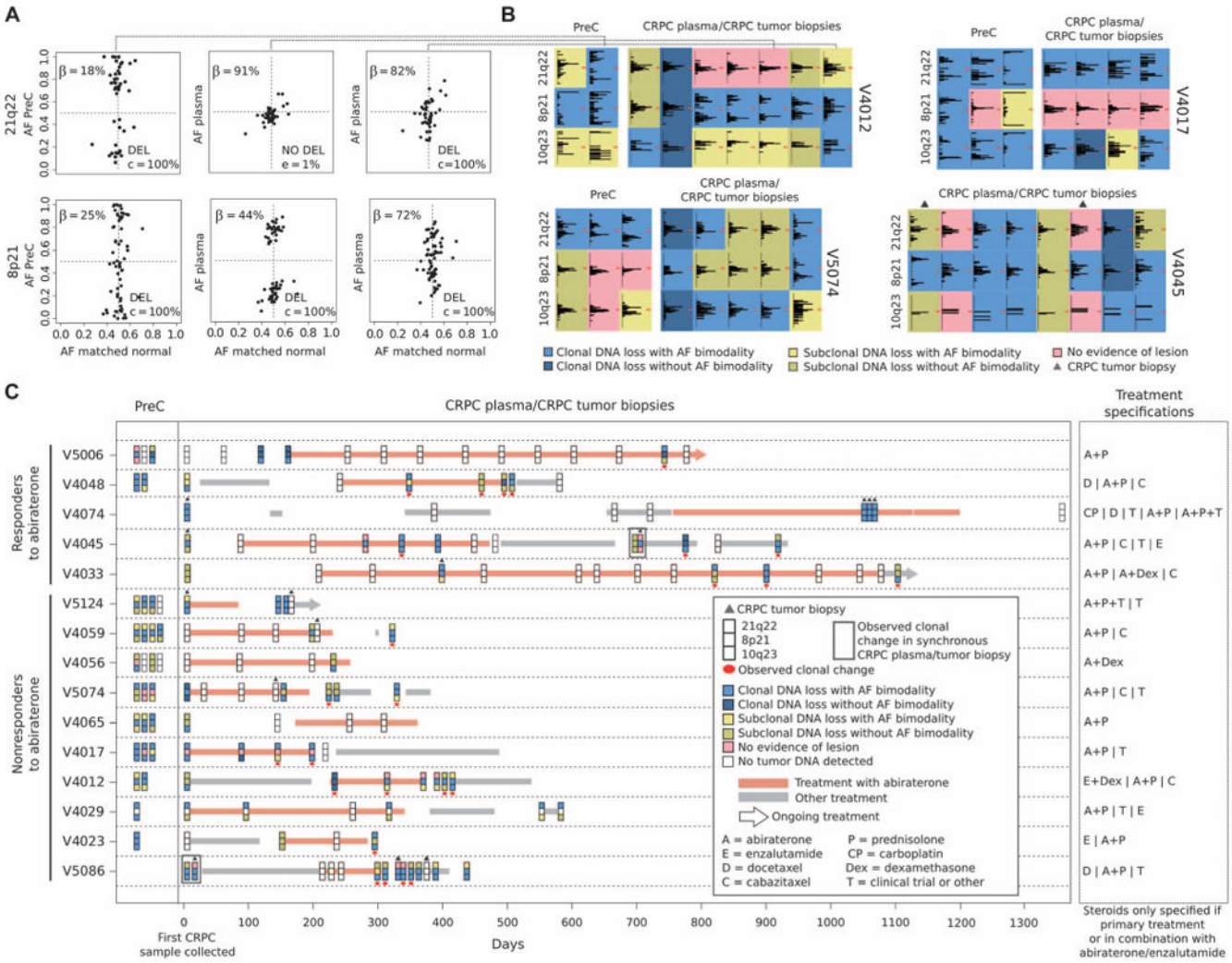

Fig. 3. Changes in clonality of deletions in precastration and sequential CRPC plasma and tumor samples

(**A**) Allelic frequency of heterozygous SNPs across 21q22 and 8p21 detected in precastration (PreC) tumor (left column) and in two plasma samples collected 17 days (middle column) and 36 days (right column) after discontinuation of abiraterone. The mono-allelic deletion at 21q, initially not detected, is subsequently present at an allelic frequency similar to the deletion at 8p. (**B**) Dominance heat maps for four patients showing clonal changes in deletions at 21q22, 8p21, and 10q23 in precastration and sequential plasma and CRPC samples. SNP allelic frequency plots in (A) and dominance heat maps in (B) connected by dotted lines are the same samples. (**C**) Temporal representation of clonal changes for deletions of 21q22, 8p21, and 10q23 in days from the first CRPC sample. Patients are divided by response to abiraterone. Horizontal bars represent time on treatment, with colored bars representing treatment with abirater-one. The chart includes 15 patients in whom tumor lesions were detected in a minimum of two CRPC samples. The panel on the right specifies the sequence of treatments administered for CRPC, divided by the "|" symbol and letters representing different drugs. Concomitant glucocorticoid administered with

enzalutamide or abiraterone is indicated (for example, A + P indicates abiraterone and prednisolone). Samples with touching borders were collected within 3 days of each other. Synchronous CRPC plasma and tumor biopsies are surrounded by a gray rectangle if a clonal change is observed. A sample is underlined by a red dot if a clonal change is observed with respect to the previous sample. For detected loss, different dominance heat map colors represent clonality status, and different color shades represent different methods used to call the loss.

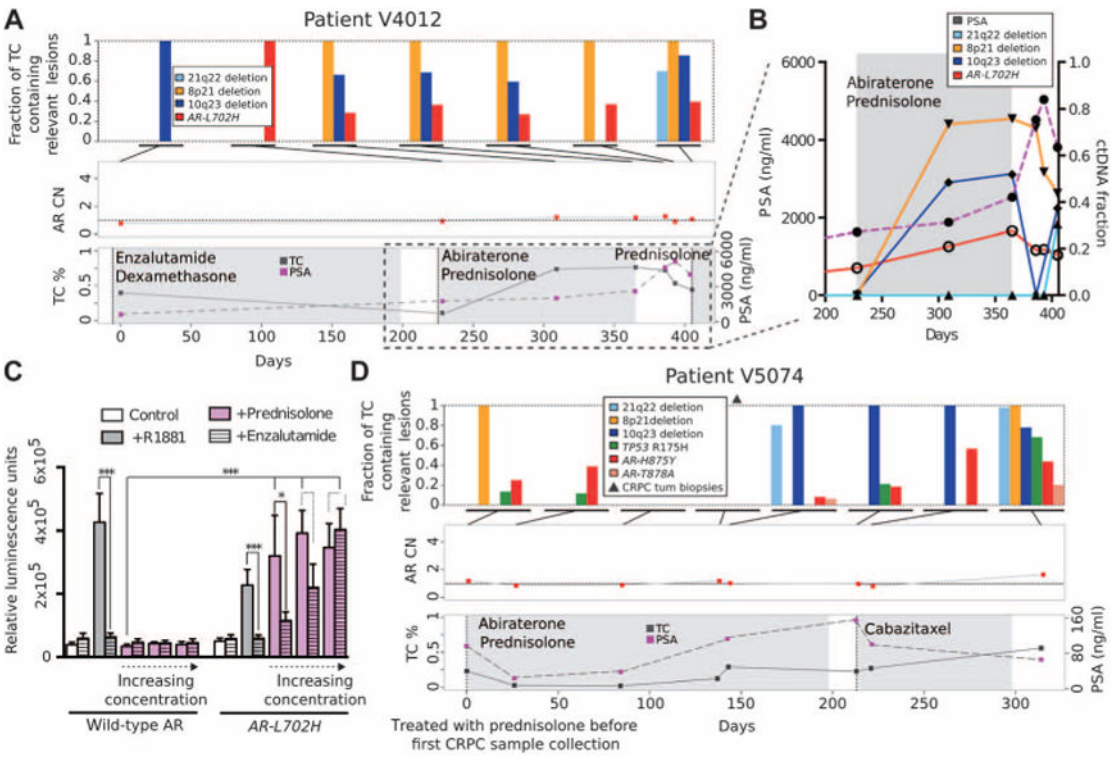

Fig. 4. *AR* point mutations associated with treatment resistance in patients receiving exogenous glucocorticoids

(**A**) These graphs show the fraction of detected tumor content (TC, estimated from the dominant lesion) containing *AR-L702H* mutation relative to coexisting genomic aberrations (upper panel), *AR* copy number (CN) state (middle panel; dashed line represents *AR* neutral copy number state), and estimated tumor content asa proportionof total circulating double-stranded DNA in sequential plasma samples, as well as PSA (lower panel) from patient V4012. Treatment with enzalutamide and dexamethasone followed by abiraterone and prednisolone is shown. Diagonal lines link bar chart representations to the time points when samples were collected, measured in days from collection of the first sample. (**B**) Inset shows changes in PSA and circulating tumor DNA (ctDNA) fractions at the start of and on treatment with abiraterone and prednisolone. (**C**) PC-3 cells cotransfected with an androgen-response element (ARE3) bound to luciferase and wild-type *AR* or *AR-L702H* were treated as shown. R1881, a synthetic androgen, was used at a concentration of 0.1 nM; enzalutamide was used at 10 μM; and prednisolone was used at 50, 100, and 500 nM. Data are from three independent experiments and represent mean and SD of 21 replicates. **P* = 0.05 to 0.01, ****P* < 0.001 [one-way analysis of variance (ANOVA) with Bonferroni correction]. Dotted lines represent no difference. (**D**) Fraction of detected tumor content containing *H875Y* and *T878A AR* mutations as a proportion of coexisting genomic aberrations, *AR* copy number, estimated tumor content, and PSA in sequential samples from patient V5074.

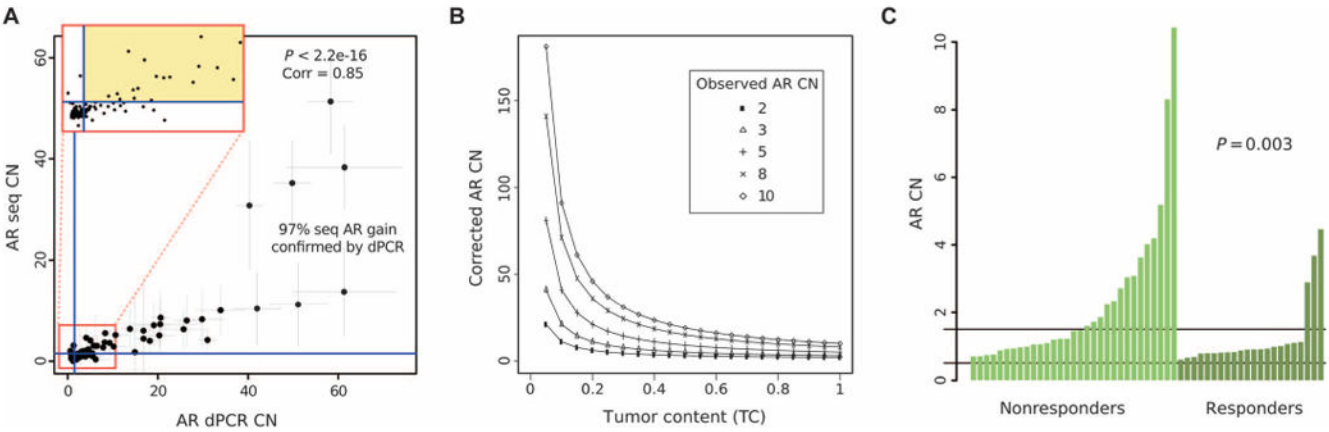

Fig. 5. Quantitation of tumor *AR* copy number in circulating tumor DNA

(**A**) Comparison of *AR* CN state inferred from target sequencing (seq) data and from digital droplet PCR (dPCR). Black dots represent combinations of CN states, and gray bars represent SDs in copy number (CN) calculation. Inset panel magnifies the highlighted area. Blue lines highlight the threshold at copy number 1.5 used for AR gain identification. Pearson correlation analysis shows evidence of statistically significant concordance between target sequencing and digital droplet PCR ($n = 128$, $P < 2.2 \times 10^{-16}$). In particular, 40 of 41 (97%) *AR* gain calls from target sequencing were confirmed by digital droplet PCR. (**B**) *AR* copy number calculated from observed *AR* copy number and corrected for tumor content. (**C**) *AR* copy number state of CRPC plasma samples collected during treatment with abiraterone from responders and nonresponders. Statistical difference between the two distributions was determined by Kruskal-Wallis statistical test ($n = 53$, $P = 0.003$).

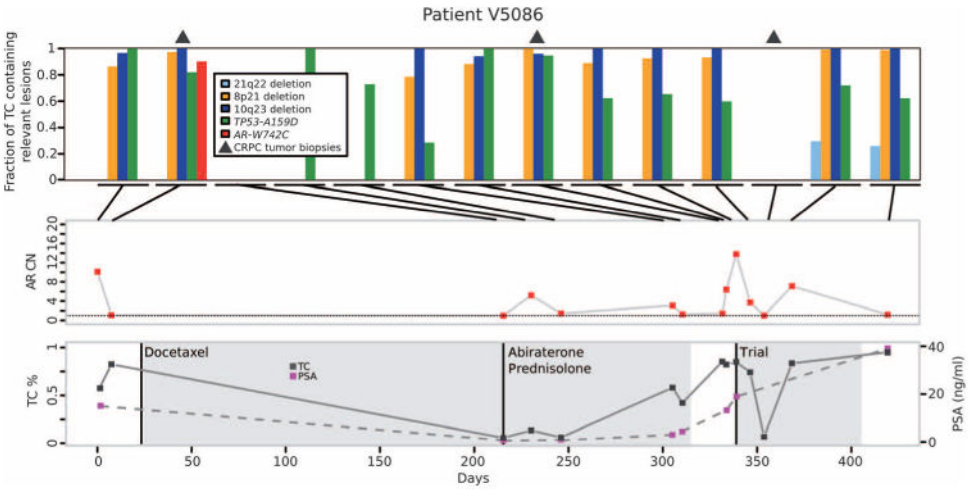

Fig. 6. Regression of independent clones with treatment-specific resistant aberrations

Top: Fraction of tumor content (TC) containing detected genomic lesions in sequential plasma and tumor samples collected after development of resistance to castration and bicalutamide for patient V5086. Diagonal lines link bar chart representations to time points when respective samples were collected, measured in days from collection of the first sample. Middle: Estimated real AR copy number (CN) status. Bottom: PSA and estimated tumor content as a proportion of total circulating DNA. An *AR-W742C* mutation was detected on biopsy of a liver metastasis but not in synchronously collected plasma, which showed *AR* copy number gain. *AR-W742C* was not detected after progression on docetaxel.

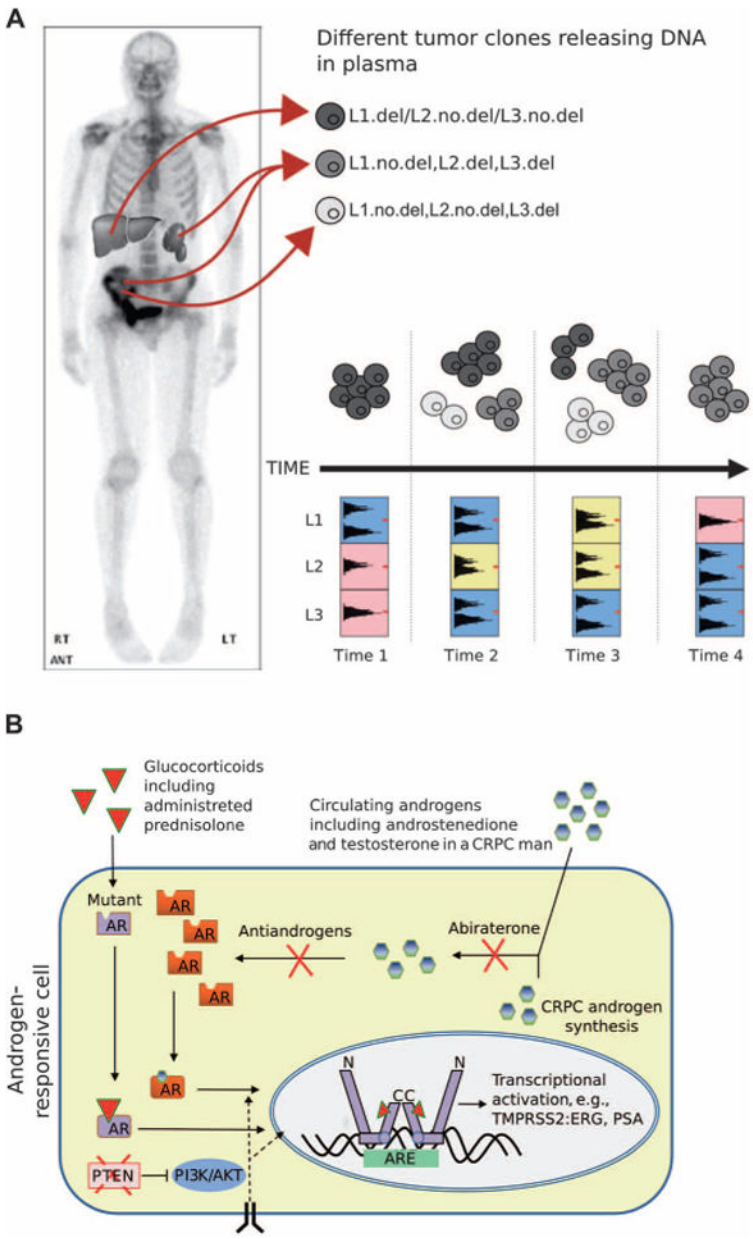

Fig. 7. Translational relevance of targeted sequencing of plasma from CRPC patients

(**A**) Schematic showing how three different tumor clones [dark gray, harboring deletion of lesion 1 (L1); gray, deletion of lesions 2 and 3 (L2 and L3); light gray, deletion of lesion 3 (L3)] released into circulation or present in metastases would be represented in dominance heat maps of copy number changes. The signal compatible with clonal mono-allelic deletion of L1 at time point 1 decreases, becoming first subclonal and then undetectable. Signal for L2 is subject to the inverse trend. L3 is identified as a dominant lesion at time points 2 and 3 because of the presence of multiple clones harboring this lesion. (**B**) Schematic showing inhibition of wild-type *AR* signaling by enzalutamide or abiraterone with bypass activation of mutant *AR* by glucocorticoids, such as exogenous prednisolone.

Sci Transl Med. Author manuscript; available in PMC 2015 May 06.

Table 1

Patient characteristics

B, bicalutamide; D, docetaxel; A, abiraterone; E, enzalutamide; PARP, poly(adenosine diphosphate–ribose) polymerase.

Patient	Precastration samples (no. of cores)	Site of castration-resistant cancer biopsy	Characteristics at first plasma draw						
			Age (years)	Metastatic sites	Previous treatment	PSA (ng/ml)	Albumin <30 g/liter	Lactate dehydrogenase >200 IU/liter	Hemoglobin <10 g/dl
V5006	3	Nil	80	Bone, lymph node	B, D	1192	No	No	Yes
V4048	2	Nil	61	Bone, lymph node	B	20	No	No	Yes
V4074	0	Penile	63	Bone, soft tissue	B, PARP inhibitor	0.22	No	Yes	No
V4045	0	Lymph node, liver	70	Bone, lymph node, lung, liver	B, D	79	No	No	No
V4033	0	Bone marrow	62	Bone, lymph node	B, D	102	No	No	No
V5124	4	Bone marrow	67	Bone	B, D, A	191	No	Yes	No
V4059	4	Bone marrow	66	Bone, lymph node	B, D	2210	No	Yes	Yes
V4056	4	Nil	72	Bone	B, D, E	12	Yes	No	No
V5074	3	Bone marrow	68	Bone	B, D	92	No	Yes	No
V4065	3	Nil	64	Bone, lymph node, lung	B, D	2500	Yes	Yes	No
V4017	3	Nil	72	Bone, lymph node	D	6.2	No	Yes	No
V4012	2	Nil	55	Bone, lymph node, liver	B, D	449	No	No	No
V4029	1	Nil	67	Bone	B, D	570	No	Yes	No
V4023	1	Nil	70	Bone, lymph node, liver	B, D	1.8	No	No	No
V5086	0	Liver	40	Bone, lymph node, liver	B	92	No	No	No
V5070	3	Nil	59	Bone, lymph nodes	B, D	67	No	No	No